applied optics

Monolithic mode separator for the first-order spatial mode of light field

Hailiang Gong,[1,2] Qing Fan,[1,2] Hai He,[1,2] Gang Li,[1,2,*] Pengfei Zhang,[1,2] and Tiancai Zhang[1,2]

[1]State Key Laboratory of Quantum Optics and Quantum Optics Devices, Institute of Opto-Electronics, Shanxi University, Taiyuan, Shanxi 030006, China
[2]Collaborative Innovation Center of Extreme Optics of the Education Ministry and Shanxi Province, Shanxi University, Taiyuan, Shanxi 030006, China
*Corresponding author: gangli@sxu.edu.cn

Received 17 December 2021; revised 27 February 2022; accepted 10 March 2022; posted 11 March 2022; published 4 April 2022

We propose a monolithic mode separator (MS) for the first-order spatial mode of a light field. The principle of the MS is an asymmetric Mach–Zehnder interferometer, which consists of two non-polarizing beam splitters, a right-angle prism, and a pentagonal prism. These optics are glued together as a monolithic one. The phase difference between the two light paths inside the interferometer is temperature controlled. The separation efficiency for two first-order orthogonal Hermite Gaussian (HG) modes, i.e., HG_{01} and HG_{10}, is 97.5%, and the overall transmission is 77%. The device is intrinsically stable and convenient to be adopted in various experiments.

https://doi.org/10.1364/AO.451255

1. INTRODUCTION

The light field with a high-order spatial mode possesses rich transverse field structures, large mode dimensions, and large orbital angular momenta (OAMs), and has been adopted in many research fields, e.g., precision measurement [1,2], quantum communication and quantum information processing [3–6], optical trapping [7,8], etc. In the field of quantum communication and quantum information processing, quantum information (qubit) is usually encoded in the transverse modes of a light field, which are orthogonal to each other. To measure quantum information, the transverse modes should be well separated and detected.

The first-order transverse mode can be separated by an asymmetric Mach–Zehnder interferometer (AMZI) [9–11] or diffraction of a fork hologram. The fork hologram can separate a light field with arbitrary transverse modes and can be easily used for simplicity. The reported highest separation efficiency (fringe visibility) and overall detection efficiency are 96.5% [12] and 27% [13], respectively. The detection efficiency is mainly limited by the low diffraction efficiency of the hologram. The AMZI is adapted from a conventional MZI by inserting rotatable a Dove prism into one arm or reflecting the beam in one arm twice [14] to reverse the beam profile along one direction. It can separate only the first-order Hermite Gaussian (HG) modes (HG_{01} and HG_{10}). Other first-order modes can be separated with the aid of modal phase shifters [15]. The separation efficiency can be as high as that of the hologram. Nevertheless, an extra locking system is usually required to maintain the phase difference between the two arms, and this makes the AMZI bulky and inconvenient to be adopted. Here we report a monolithic mode separator (MS) for the first-order spatial mode of a light field. The phase difference is temperature controlled, and the performance is comparable to one with separate optics. The AMZI is compact and conveniently adopted for various applications.

2. THEORY

As we know, first-order OAM light fields can form a two-dimensional Hilbert space. The density matrix $\hat{\rho}$ of any single quantum state can be represented by three Stokes parameters (S_1, S_2, S_3) [16]:

$$\hat{\rho} = \frac{1}{2}\sum_{i=0}^{3} s_i \hat{\sigma}_i, \tag{1}$$

where $\hat{\sigma}_i$ is the Pauli matrix along the three axes of the Bloch sphere. The Stokes parameter of the light field on a Poincaré sphere is equivalent to the quantum state on a Bloch sphere as shown in Fig. 1. The Stokes parameters can be deduced from the light intensity of different modes as

$$\begin{aligned} S_0 &= I_{\mathrm{HG}_{10}} + I_{\mathrm{HG}_{01}}, \\ S_1 &= I_{\mathrm{HG}_{10}} - I_{\mathrm{HG}_{01}}, \\ S_2 &= I_{\mathrm{HG}_{10}^{45^\circ}} - I_{\mathrm{HG}_{10}^{135^\circ}}, \\ S_3 &= I_{\mathrm{LG}_0^{+1}} - I_{\mathrm{LG}_0^{-1}}, \end{aligned} \tag{2}$$

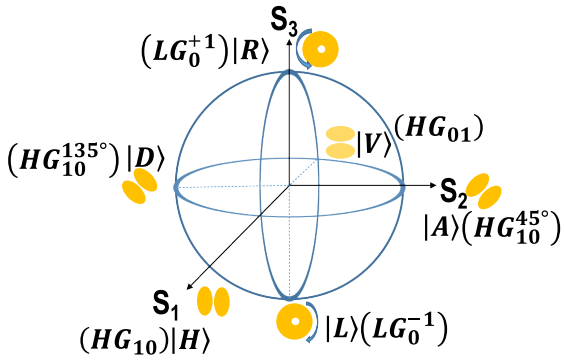

Fig. 1. Poincaré sphere with first-order orbital angular momentum.

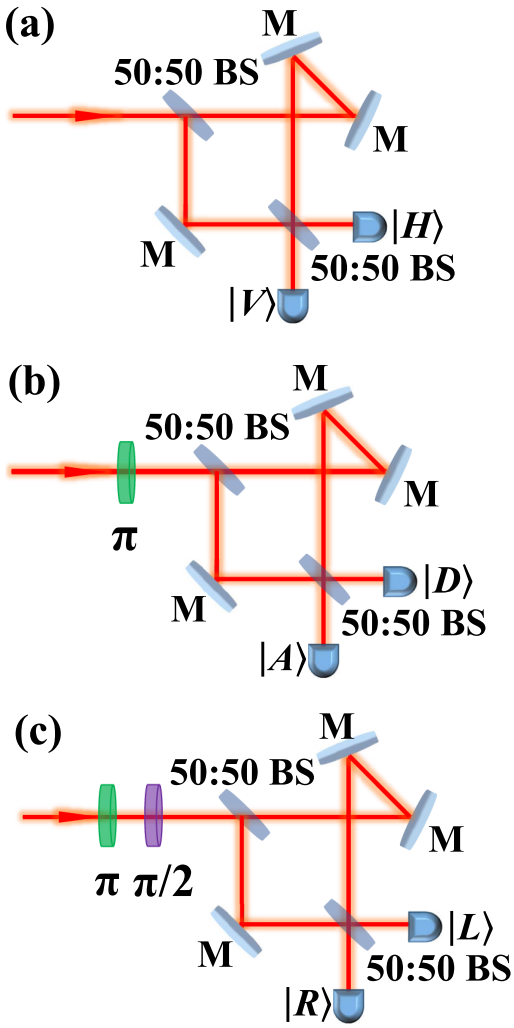

Fig. 2. Measurements of (a) $\hat{S}_0$ and $\hat{S}_1$, (b) $\hat{S}_2$, and (c) $\hat{S}_3$. M, mirror; 50:50 BS, symmetric non-polarizing beam splitter. The π phase shifter usually is a Dove prism. The $\pi/2$ phase shifter could be constructed using a pair of cylindrical lenses with lens separations given by $\sqrt{2}f$; f is the focal length of the cylindrical lenses.

where I is the light intensity of the fiducial mode. Thus, the Stokes parameter can be measured by the MS with the aid of necessary mode converters (see Fig. 2).

In Fig. 2, the mode converters (π and $\pi/2$ phase shifters) are usually constructed by a Dove prism and a pair of cylindrical lenses, respectively. The AMZI alone can separate only HG_{10} and HG_{01} modes and measure $\hat{S}_0$ and $\hat{S}_1$ [see Fig. 2(a)]. The 45° or 135° HG_{10} mode ($\pm LG_{01}$ modes) is first converted to HG_{01} or HG_{10} mode by a $\pi(\pi/2)$ phase shifter and then separated by the AMZI. Therefore, $\hat{S}_2$ and $\hat{S}_3$ can be measured [(b) and (c) in Fig. 2].

3. DESIGN OF THE MONOLITHIC MS

The schematic of the AMZI invented in our paper is shown in Fig. 3(a). The input beam is separated into two paths by the first 50:50 non-polarizing beam splitter (NPBS), and then the two beams are reflected by a right-angle prism and a pentagonal prism. Finally, the two beams interfere on the second 50:50 NPBS. The size and the materials of each optics are shown in Table 1. All the optics are machined with high precision and glued together as a monolithic part. The monolithic AMZI is housed in a copper-made oven, and the temperature is precisely controlled by a temperature controller (TEC Source 5240, Arroyo Instruments) via a Peltier plate [see Fig. 3(b)]. The temperature fluctuation of the whole setup is below 0.01°C. Thus, by taking account of the thermal expansion coefficient $\alpha = 7.1 \times 10^{-6}$°C, refractive index $n = 1.5$ of the glass material H-K9L, as well as the path difference 24 mm between the two arms, we can get that the phase stability between the two arms is blow 1° for the 852 nm light field. The phase difference can also be precisely tuned by the temperature.

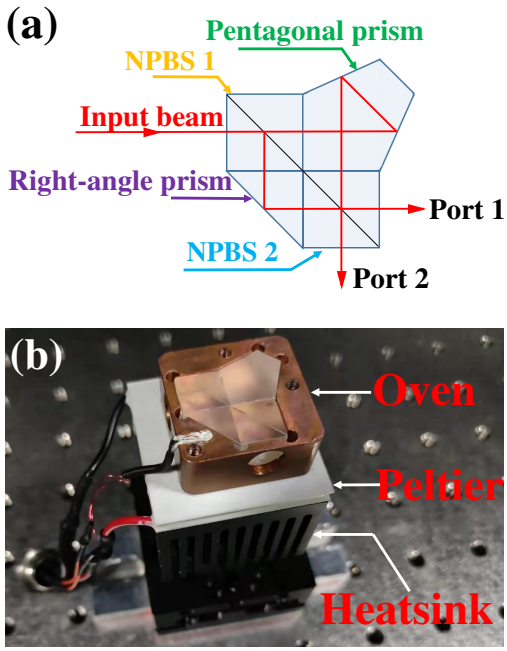

Fig. 3. Schematic diagram of the (a) AMZI and (b) a picture of the real device. In (a), the input beam is separated into two paths by the first 50:50 non-polarizing beam splitter (NPBS1), and then the two beams are reflected by a right-angle prism and a pentagonal prism. Finally, the two beams interfere on 50:50 NPBS2. The material of these optics is H-K9L. In (b), in addition to the internal optics, it also includes a copper-made oven, Peltier plate, and heatsink.

Table 1. Parameters of AMZI Components

Name	Material	Size (mm)
NPBS	H-K9L	10
Pentagonal prism	H-K9L	10
Right-angle prism	H-K9L	10

4. PERFORMANCE OF THE MS

The MS (AMZI) is first tested by a beam with fundamental mode LG_{00}. The beam has a waist of 0.35 mm and is aligned to the AMZI. Transmission port 1 versus the temperature is shown in Fig. 4 with the temperature changing from 18°C to 26°C. An interference fringe with visibility of about 96.6% is obtained. We can also get that a π-phase difference can be obtained by tuning the temperature of 0.9°C. A maximum transmission of 76.8% for the fundamental mode can also be achieved. It is mainly limited by the residual reflection of the anti-reflective coatings associated with every optic.

To characterize the performance of the device for first-order OAM light fields, a series of well-defined HG_{10}-mode, 45° HG_{10}-mode, and LG_{01}-mode laser fields is generated and used to test the MS. The three light fields are eigen-states of the three Stokes parameters $\hat{S}_1$, $\hat{S}_2$, and $\hat{S}_3$, respectively. The HG_{10} light field is generated by sending a light beam with the fundamental mode LG_{00} through the π phase plate (PE-202, HOLO/OR) and then filtered by a Fabry–Perot cavity. Thus, a high-purity HG_{10} mode field is obtained. The HG_{10} mode is converted to LG_{01} mode through the integrated cylindrical lens [17]. The corresponding beam waists for the HG_{10} mode and LG_{01} mode are 0.6 mm and 0.56 mm, respectively.

By carefully aligning the incident angle of the first-order OAM light fields to the AMZI, the HG_{10}-mode light field shows interference fringes at the output ports when the phase difference between the two arms inside the AMZI is tuned by changing the temperature. The fringe is shown in Fig. 5(a). The visibility of the interference fringe is 97.5%, which means that the two orthogonal modes HG_{10} and HG_{01} can be separated with high efficiency when the phase difference is maintained at zero or π. Figures 5(b) and 5(c) show transmission versus phase

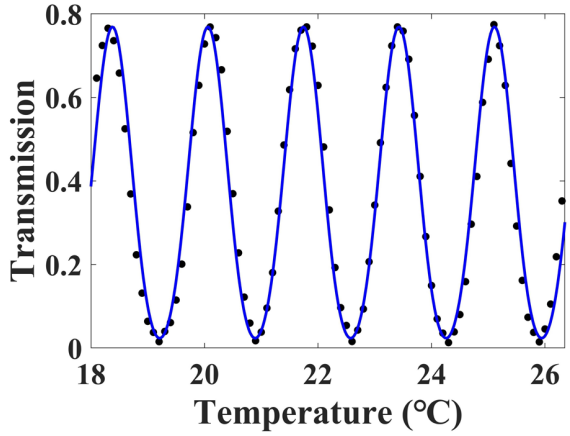

Fig. 4. LG_{00} interference result from port 1. The LG_{00} mode with a beam waist of 0.35 mm is aligned to the AMZI, then interferes when the temperature is tuned from 18°C to 26°C. The highest transmission of AMZI is 76.2%, and interference fringe has a visibility of about 96.6%. The solid line is the fitting with a trigonometric function.

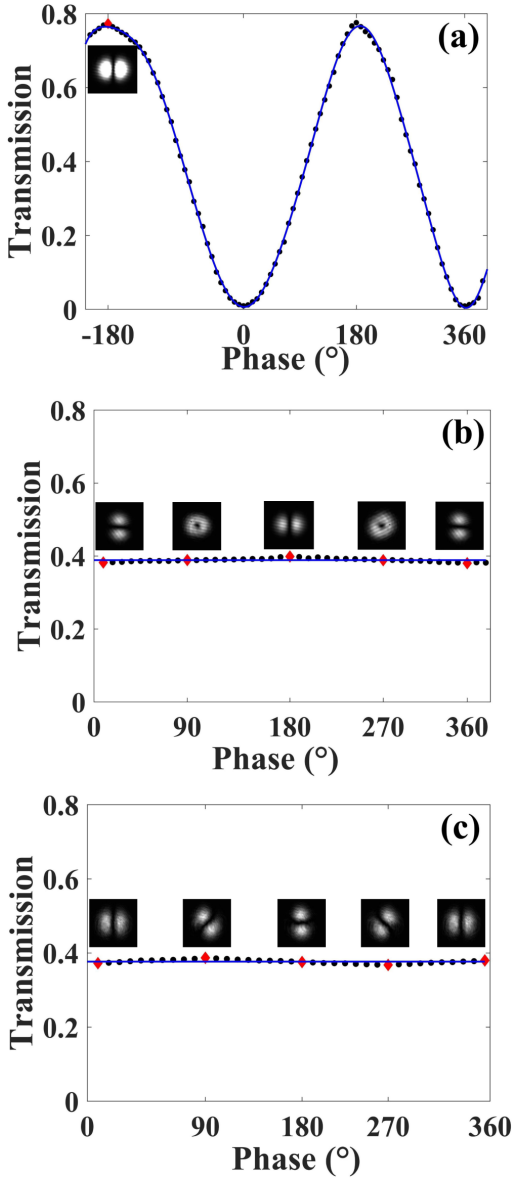

Fig. 5. AMZI interference results from port 1 with light fields of (a) HG_{10} mode, (b) 45° HG_{10} mode, and (c) LG_{01} mode. The pictures of the output field are given at the position of the red data points. The visibilities of the fringes are (a) 97.5%, (b) 2.6%, and (c) 3.2%. The maximum transmission of HG_{10} mode is 77.6%. The line in (a) is the fitting with trigonometric function, and lines in (b) and (c) represent the average value of the corresponding data.

difference with the incident beam in 45° HG_{10} mode and LG_{01} mode, respectively. Images of the output beam profile with a phase difference at zero, $\pi/2$, π, $3\pi/2$, and 2π are also shown. The visibilities of the two fringes are 2.6% and 3.2%, which are close to theoretical zero.

Then, we set the phase difference at π and observe the output light field by rotating the angle of the incident mode so that the mode is changing along the equator of the Poincaré sphere with the aid of a Dove prism (PS992M-B, Thorlabs). The dependance of output light transmission versus mode angle is displayed in Fig. 6, which also shows an interference fringe with visibility

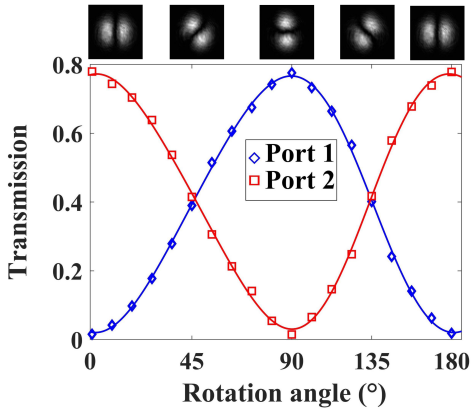

Fig. 6. Output of AMZI with the rotation of input HG_{10} mode. The phase difference inside the AMZI is kept as π. The pictures on the top show the input HG_{10} mode aligned in angles of 0°, 45°, 90°, 135°, and 180°. The visibility of fringe is 96%. The transmissions of the two ports vary with the rotation angle of the HG_{10} mode, and the highest transmissions of both ports are about 77.5%. The lines are the fitting with trigonometric function.

of 96%. This means that our device can separate the HG_{10} and HG_{01} modes with cross talk below 19 dB.

Finally, to characterize the overall transmission efficiency and stability of the device, the output intensities from both outports are recorded for 4 h with input mode HG_{10} and with the phase difference is set at $\pi/2$ and π. The data are summarized in Fig. 7. The overall transmission is measured as 77.2%, which is similar to that of the fundamental mode. The output fluctuation is below 0.3% within 4 h, and the precision of temperature control is 0.01°C.

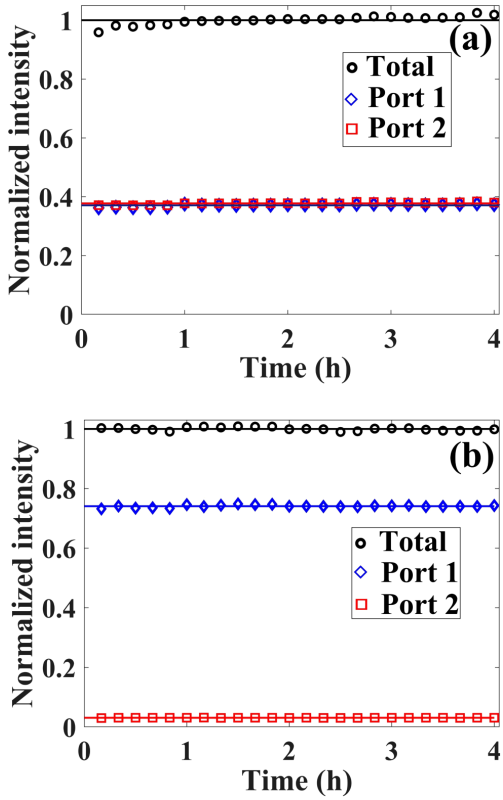

Fig. 7. Output power stability in time with the phase set as (a) $\pi/2$ and (b) π. The output intensities from both outports are recorded for 4 h with the input mode HG_{10}. The overall transmission is 77.2%, and the output power fluctuation is below 0.3%. The precision of temperature control is 0.01°C. The lines are the average values for different sets of data.

5. DISCUSSION

The two beams travel with different distances within the AMZI; one beam propagates 24 mm longer than the other beam before they interfere on the second NPBS. Therefore, the visibility of the fringe would be dramatically suppressed for a very small beam waist. To analyze the effect, we assume a perfect HG_{10} light field:

$$E_{10}(x,y,z)=\frac{2\sqrt{2}x}{\sqrt{\pi}\times\omega(z)^2}\exp\left[-\left(x^2+y^2\right)/\omega(z)^2\right]\times\exp\left[-ik\left(z+\frac{x^2+y^2}{2R(z)}\right)+i2\arctan\frac{z}{z_R}\right], \quad (3)$$

with its waist exactly at the position ($z=0$) of the splitting surface of the first NPBS. The two beams after the NPBS propagate $d1=20$ mm and $d2=44$ mm inside the AMZI and interfere on the second NPBS. The intensity at one outport of the AMZI can be obtained by

$$I=\frac{1}{2}\iint\left[E_{10}(x,y,nd1)+E_{10}(x,y,nd2)\right]\times\left[E_{10}(x,y,nd1)+E_{10}(x,y,nd2)\right]^{*}\mathrm{d}x\mathrm{d}y, \quad (4)$$

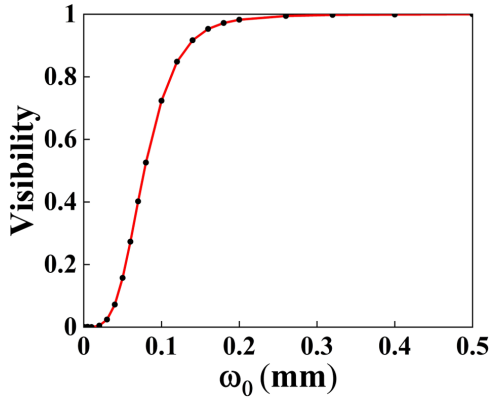

Fig. 8. Theoretical calculation of the visibility of the fringe for HG_{10} mode. One beam propagates 24 mm longer than the other beam before they interfere on the second NPBS in AMZI. ω_0 is the waist of the light field.

with n the refractive index of glass. Then the visibility of the fringe can be obtained by varying the phase difference. The dependence of visibility on the size of the beam waist is shown in Fig. 8. We can see that visibility over 95% can be achieved as long as the size of the beam waist is bigger than 0.16 mm.

6. CONCLUSION

In conclusion, we have demonstrated a monolithic AMZI for separation of the first-order OAM light field. The separation efficiency is 97.5% for HG_{01} mode and HG_{10} mode, and the transmission efficiency is 77% with cross talk below 19 dB. The parameters of our device are better than other solutions to separate OAM light fields, such as fork holograms. In addition, our device is compact and does not need an accessary locking loop. The phase of the AMZI can be tuned with resolution below 1° by controlling the temperature. The device can serve as a simple optics for the research of quantum information processing with the first-order OAM light field.

Funding. National Key Research and Development Program of China (2017YFA0304502); National Natural Science Foundation of China (11634008, 11974223, 11974225); Fund for Shanxi "1331 Project" Key Subjects.

Disclosures. The authors declare no conflicts of interest.

Data availability. Data underlying the results presented in this paper are not publicly available at this time but may be obtained from the authors upon reasonable request.

REFERENCES

1. D. Deng, M. Lin, Y. Li, and H. Zhao, "Precision measurement of fractional orbital angular momentum," Phys. Rev. Appl. **12**, 014048 (2019).
2. S. Xiao, L. Zhang, D. Wei, F. Liu, Y. Zhang, and M. Xiao, "Orbital angular momentum-enhanced measurement of rotation vibration using a Sagnac interferometer," Opt. Express **26**, 1997–2005 (2018).
3. D.-S. Ding, W. Zhang, Z.-Y. Zhou, S. Shi, G.-Y. Xiang, X.-S. Wang, Y.-K. Jiang, B.-S. Shi, and G.-C. Guo, "Quantum storage of orbital angular momentum entanglement in an atomic ensemble," Phys. Rev. Lett. **114**, 050502 (2015).
4. X. Yin, H. Chang, X. Cui, J.-X. Ma, Y.-J. Wang, G.-H. Wu, L. Zhang, and X. Xin, "Adaptive turbulence compensation with a hybrid input–output algorithm in orbital angular momentum-based free-space optical communication," Appl. Opt. **57**, 7644–7650 (2018).
5. Y. Zhang, I. B. Djordjevic, and X. Gao, "On the quantum-channel capacity for orbital angular momentum-based free-space optical communications," Opt. Lett. **37**, 3267–3269 (2012).
6. D. S. Simon, C. A. Fitzpatrick, and A. V. Sergienko, "Discrimination and synthesis of recursive quantum states in high-dimensional Hilbert spaces," Phys. Rev. A **91**, 043806 (2015).
7. F. K. Fatemi and M. Bashkansky, "Cold atom guidance using a binary spatial light modulator," Opt. Express **14**, 1368–1375 (2006).
8. J. Poulin, P. S. Light, R. Kashyap, and A. N. Luiten, "Optimized coupling of cold atoms into a fiber using a blue-detuned hollow-beam funnel," Phys. Rev. A **84**, 053812 (2011).
9. J. Leach, J. Courtial, K. Skeldon, S. M. Barnett, S. Franke-Arnold, and M. J. Padgett, "Interferometric methods to measure orbital and spin, or the total angular momentum of a single photon," Phys. Rev. Lett. **92**, 013601 (2004).
10. V. Delaubert, N. Treps, M. Lassen, C. C. Harb, C. Fabre, P. K. Lam, and H.-A. Bachor, "TEM_{10} homodyne detection as an optimal small-displacement and tilt-measurement scheme," Phys. Rev. A **74**, 053823 (2006).
11. J. Guo, C. Cai, L. Ma, K. Liu, H. Sun, and J. Gao, "Measurement of stokes-operator squeezing for continuous-variable orbital angular momentum," Sci. Rep. **7**, 4434–4443 (2017).
12. A. Nicolas, L. Veissier, L. Giner, E. Giacobino, D. Maxein, and J. Laurat, "A quantum memory for orbital angular momentum photonic qubits," Nat. Photonics **8**, 234–238 (2013).
13. A. Nicolas, L. Veissier, E. Giacobino, D. Maxein, and J. Laurat, "Quantum state tomography of orbital angular momentum photonic qubits via a projection-based technique," New J. Phys. **17**, 033037 (2015).
14. C. Cai, L. Ma, J. Li, H. Guo, K. Liu, H. Sun, and J. Gao, "Experimental characterization of continuous-variable orbital angular momentum entanglement using stokes-operator basis," Opt. Express **26**, 5724–5732 (2018).
15. M. T. L. Hsu, W. P. Bowen, and P. K. Lam, "Spatial-state stokes-operator squeezing and entanglement for optical beams," Phys. Rev. A **79**, 043825 (2009).
16. A. F. Abouraddy, A. V. Sergienko, B. E. Saleh, and M. C. Teich, "Quantum entanglement and the two-photon Stokes parameters," Opt. Commun. **201**, 93–98 (2002).
17. J. Jia, Q. Li, K. Zhang, D. Chen, C. Wang, H. Gao, F. Li, and P. Zhang, "Integrated design of pi/2 converter and its experimental performance," Appl. Opt. **57**, 6076–6082 (2018).